NOVEL ELECTRODE GEOMETRY FOR ELECTROSTATIC ENERGY CONVERSION WITH TUNING CAPABILITY

Daniel Hoffmann[1*], B. Folkmer[1], Y. Manoli[1, 2]
[1] HSG-IMIT – Institute of Micromachining and Information Technology, VS-Villingen, Germany
[2] Fritz-Huettinger Chair of Microelectronics, Department of Microsystems Engineering – IMTEK, University of Freiburg, Germany
*Presenting Author: Daniel.Hoffmann@hsg-imit.de

Abstract: This paper reports on the implementation of triangular electrodes for electrostatic energy conversion in a continuous system. We successfully designed and manufactured electrostatic transducer devices based on silicon MEMS fabrication technology. The use of triangular structures for implementing variable capacitive electrodes is a further development of our continuous work on in-plane electrostatic energy harvesting devices. This kind of geometry has not yet been considered for electrostatic energy conversion by other research groups. In this paper we present results from experimental characterization of electrostatic transducers with triangular electrodes.

Keywords: Energy harvesting, electrostatic vibration transducer, electrode geometry

INTRODUCTION

The electrostatic transduction mechanism, which is one of the three principles used for energy conversion from vibrations, may be implemented in a variety of different ways [1], [2]. In contrast to the electromagnetic conversion mechanism, not only the spatial arrangement of the transducer elements but also the electrical context is variable [1]. In line with our continuous development of electrostatic MEMS energy harvesting devices, this paper focuses on the transducer type, which is implemented in a continuous operation scheme using two variable capacitors [3]. The realization of the variable capacitors is strongly dependent on the technology available. Based on a fabrication process developed earlier, an in-plane architecture incorporating a single device layer is used [3]. For this configuration different electrode geometries may be realized resulting in different characteristics for the capacitance change per unit displacement [4]. Very common electrode geometries include the area-overlap and the gap-closing design. In this paper we present experimental data obtained from a triangular electrode design. The potential for energy harvesting applications is discussed and disadvantages highlighted.

DESIGN & FABRICATION

Transducer structure

The transducer structure, schematically outlined in fig. 1, consists of a seismic mass suspended by four folded beam springs and the electrode elements. The device layer thickness is 50 µm and the displacement amplitude x_{max} is limited to 20 µm by mechanical stoppers. The active devices size (transducer layout area) is 3.5 mm x 4.5 mm. A detailed description of the fabrication process is given in [3].

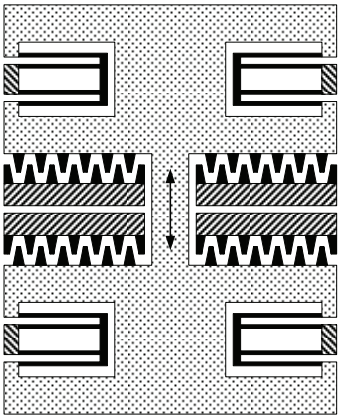

Fig. 1: Schematic view of the transducer structure incorporating triangular electrodes.

Electrode geometry

The triangular electrode geometry is shown in fig. 2. The design requires some consideration with respect to both manufacturing and operation. The initial gap g_0 at x=0 must not be smaller than the minimum feature size that can be fabricated with the manufacturing facilities available. Furthermore, the minimum gap g_{min} at x=x_{max} should not be too small in order to avoid voltage breakdowns between the electrodes. The general relation between the displacement x and the gap g between the electrodes is given by equation 1:

$$g(x) = \left(\frac{g_{min}}{\sin(\alpha)} + x_{max} - x \right) \cdot \tan(\alpha) \cdot \cos(\alpha) \quad (1)$$

where α is the angle of the side wall (see fig. 2). In this design study we have chosen an angle of 5.71°, which corresponds to tan(α)=0.1. Furthermore, we have set the minimum gap g_{min} to 0.4 µm. As a result, the initial gap g_0 yields 2.4 µm, which is the minimum feature size that we can reliably produce in a device layer of 50 µm. Relevant parameters are summarized in table 1.

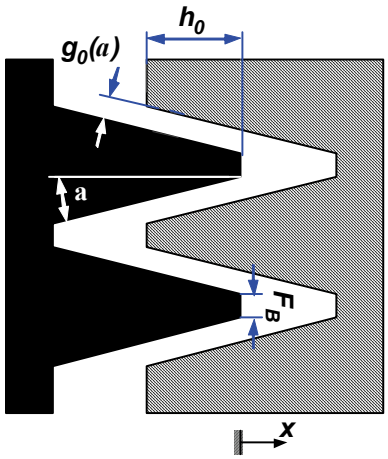

Fig. 2: Schematic view of the electrode geometry.

Table 1: Design Parameters.

Parameter	Value	Unit
Chip length	7	mm
Chip width	6	mm
Mass of proof mass	960	µg
Displacement limit	20	µm
Number of electrodes	1217	1
Side wall angle	5.71	°
Initial gap g_0	2.4	µm
Minimum gap g_{min}	0.4	µm

Harvesting Circuit

The electrostatic vibration transducers have been characterized using two different circuits. A more general characterization of the device behavior was carried out using a symmetric circuit C1 with two load resistors (fig. 3a). In this electrical context, AC output voltage and AC output power was measured for different excitation amplitudes over a defined frequency band. The influence of the bias voltage was investigated at constant excitation amplitude. The DC output performance was characterized using a circuit C2 with a full-bridge rectifier and an energy storage element (fig. 3b). A load resistor is continuously connected to the storage capacitor to simulate a consumer.

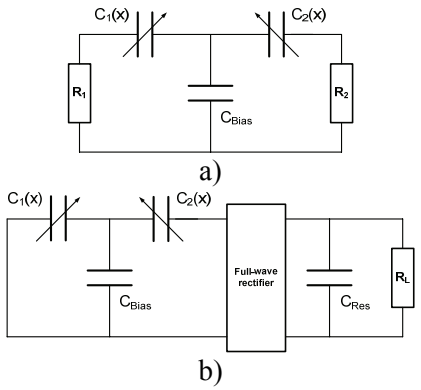

Fig. 3: Electrical context: a) symmetric circuit with two load resistors; b) circuit with full-bridge rectifier, energy storage capacitor and load resistor.

EXPERIMENTAL CHARACTERISATION

The electrostatic harvesting devices were characterized on a labshaker (TIRA GmbH), which is operated in a feedback control loop. The voltage is measured using a data acquisition system (NI).

In fig. 4 the RMS voltage output (over R_1) is shown for different excitation amplitudes. With increasing device excitation the frequency response becomes more and more nonlinear approaching a strong softening characteristic. The voltage peaks shift towards lower frequencies when the excitation is increased. For a bias voltage of 10 V the output voltage is between 0.2 V and 0.7 V when a load resistance of 820 kΩ is used.

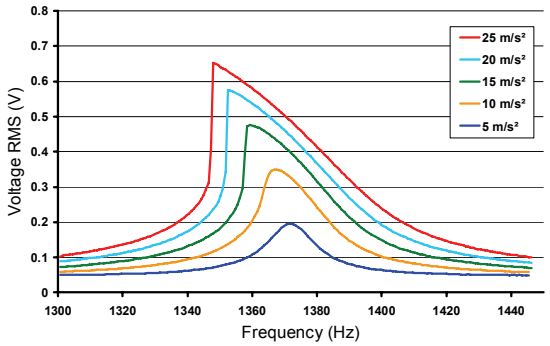

Fig. 4: AC RMS voltage for different excitation amplitudes. Bias voltage: 10 V, Load: 820 kΩ

The corresponding RMS power output is shown in fig. 5a. From an input acceleration of 25 m/s² a power of 0.5 µW can be harvested. Considering the load resistor R_2 a total power of 1 µW is converted.

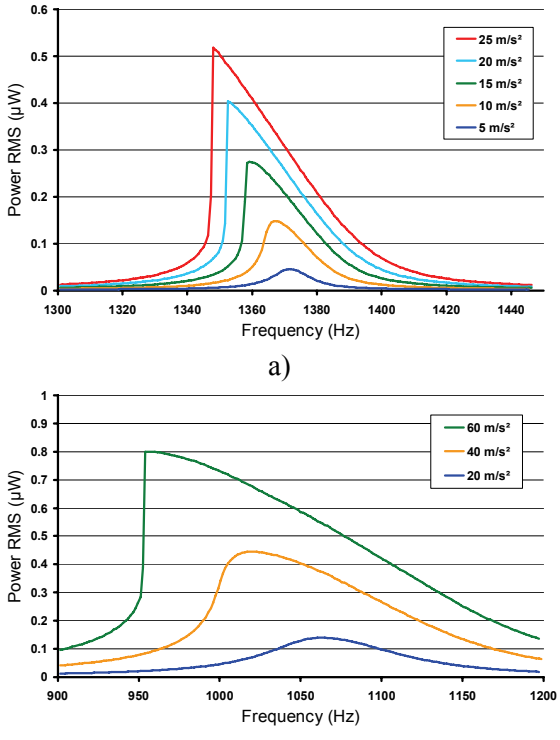

Fig. 5: AC RMS power for different excitation amplitudes. Load resistance: 820 kΩ. a) Bias voltage: 10 V, b) Bias voltage: 25 V.

The output power for a higher bias voltage is shown in fig. 5b. When the bias voltage is increased at constant excitation amplitude the power output drops (Compare: 0.4 µW at 20 m/s² and 10 V (fig. 5a) and 0.15 µW at 20 m/s² and 25 V (fig. 5b)). However, at higher bias voltages higher acceleration amplitudes can be applied resulting in higher power output (0.8 µW at 60 m/s²).

What seems interesting is the impression that the frequency response broadens significantly if higher bias voltages are used. For an acceleration amplitude of 40 m/s² a half bandwidth of 140 Hz is obtained (fig. 5b). Using a bias voltage of 10 V the bandwidth is below 30 Hz (fig. 5a). However, higher bias voltages require greater excitation levels.

In fig. 6 the power output is shown for different bias voltages. There is a strong influence of the bias voltage on the resonance frequency, which shifts towards lower values with increasing bias voltage. From fig. 6 it is evident, that the power output decreases for increasing bias voltages (constant excitation) due to a strong increase of electro-mechanical coupling, which reduces the displacement amplitude of the proof mass. A maximum is obtained for an optimum bias voltage of about 10 V if the excitation amplitude is 20 m/s² (fig. 6a). For voltages below 10 V the displacement amplitude approaches the displacement limit due to further reduced coupling and thus impacts occur between the proof mass and the mechanical stoppers. With increasing excitation amplitudes the optimum bias voltage raises (fig. 6b: 15 V at 40 m/s²).

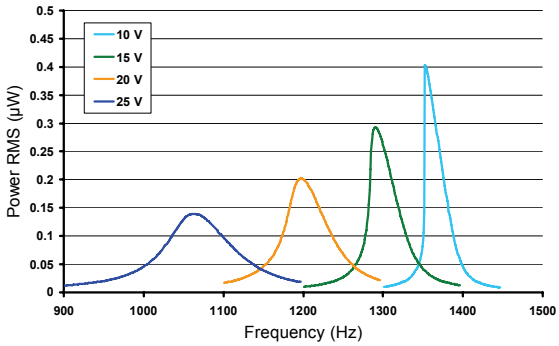

a)

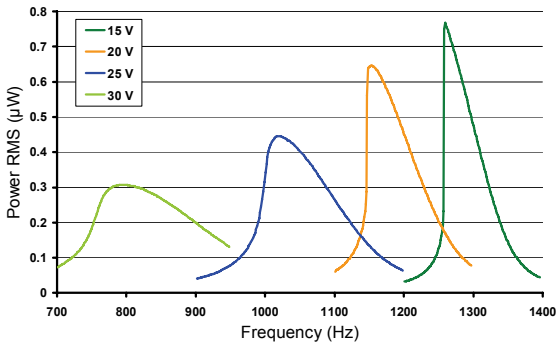

b)

Fig. 6: AC RMS power output for different bias voltages. Load resistance: 820 kΩ. a) Excitation amplitude: 20 m/s², b) Excitation amplitude: 40 m/s².

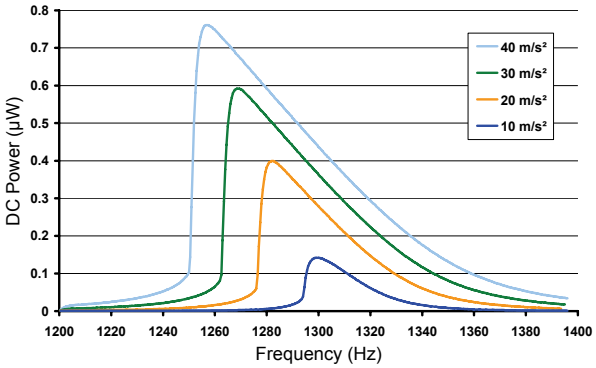

Fig. 7: DC power output for different excitation amplitudes. Bias voltage: 15 V, Load: 800 kΩ

The strong dependency of the resonance frequency on the bias voltage provides an opportunity for tuning the resonance frequency of the device. In this way, the bias voltage can be adjusted in such a manner, that the resonance frequency is matched to the dominant frequency of the vibration source. Although the power reduces with increasing bias voltage, the effectiveness is still far higher than operating the device beside the resonance frequency.

In the following, experimental results are shown using circuit C2, which includes a full-bridge rectifier and a capacitor storage element (fig. 3b). Fig. 7 shows the DC power output at the load resistor R_L for different excitation amplitudes. In general, the frequency response curves do not diverge significantly from the curves obtained with circuit C1. Using a bias voltage of 15 V a power output of 0.4 µW is obtained for an excitation amplitude of 20 m/s².

The influence of the bias voltage on the output power is shown in fig. 8. Comparing the results to fig. 6a a significant difference can be observed. There exists an optimum bias voltage (15 V) at which the peak power becomes maximal. For bias voltages lower or higher than 15 V the power drops. However, at a bias voltage of 10 V the power output increases significantly and the frequency response curve shows a broader bandwidth. It is assumed that the proof mass oscillates against the limit stop (impact mode). Though, it is not clear why the power output increases by a factor of more than two if the bias voltage is decreased from 12 V to 10 V.

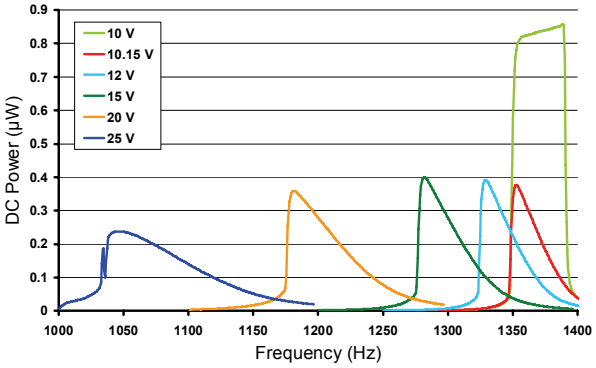

Fig. 8: DC power output for different bias voltages. Excitation amplitude: 20 m/s², Load: 800 kΩ

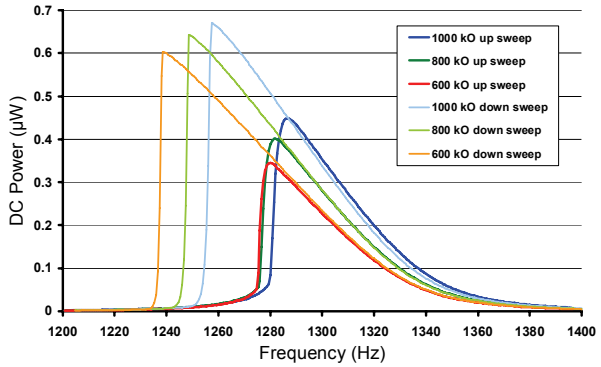

Fig. 9: DC power output for frequency up-sweeps and down-sweeps at different load resistances. Bias voltage: 15 V, Excitation amplitude: 20 m/s²

In fig. 9 the frequency response is shown for frequency up-sweeps and down-sweeps. A strong non-linear device characteristic with softening behavior is observable. Performing a down-sweep allows to reach the curved peak of the frequency response function resulting in larger power outputs. However, the amplitude in this branch is not stable and perturbations of the input vibration amplitude, as usually present in realistic vibration profiles, will cause the amplitude to drop down to the lower branch resulting in a strongly reduced energy conversion effectiveness.

The charging response of the energy storage capacitor (fig. 3b) is shown in fig. 10. Charging is carried out for different load resistances, while the load resistor is continuously connected to the capacitor. The charging time is approximately 10 s for a capacitor with a capacitance of 2 µF and an excitation of 30 m/s². The bias voltage was 15 V.

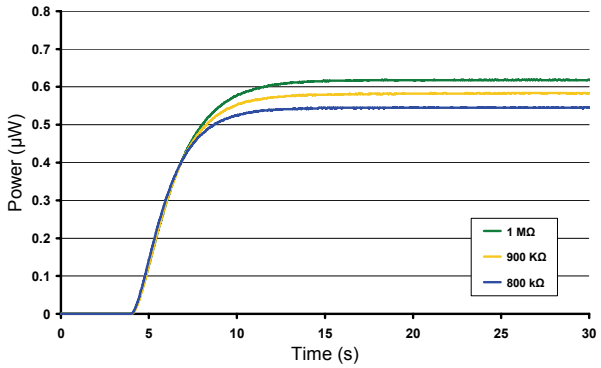

Fig. 10: Charging response of the energy storage capacitor (2 µF) at different load resistances. Bias voltage: 15 V, Excitation amplitude: 30 m/s².

CONCLUSION

A triangular electrode geometry was designed for incorporation into an electrostatic in-plane MEMS energy converter. The device is implemented in a continuous system using two complementary capacitors. For characterization of the device behavior prototypes were fabricated using MEMS fabrication technologies. Characterization was carried out using two different energy harvesting circuits whereas one circuit includes a full-bridge rectifier and an energy storage capacitor.

In general, experimental data shows a strong non-linear frequency response with softening characteristic. Output voltages range between 0.2 V_{RMS} and 0.8 V_{RMS} using bias voltages between 10 V and 25 V. The corresponding power output ranges between 0.1 µW and 0.8 µW.

Due to the non-linear capacitance change per unit displacement of the triangular electrode geometry the resonance frequency is strongly dependent on the bias voltage. This effect may be used for tuning purposes in order to match the resonance frequency of the device to the dominant frequency present in the application. By increasing the bias voltage from 10 V to 25 V the resonance frequency can be shifted from 1360 Hz down to 1060 Hz.

At a constant excitation amplitude of 20 m/s² the maximum output power is achieved with a low bias voltage of 10 V. An increase of the bias voltage causes a reduction of the power output (power drops by a factor of 2.7 if the bias voltage is increased by 15 V).

The use of a circuit with rectifier and energy storage changes the device behavior with respect to the influence of the bias voltage. If the impact mode is ignored for the time being the optimum bias voltage shifts from 10 V to 15 V (20 m/s²). A further reduction of the bias voltage leads to a decrease of the power output. However, at a bias voltage of 10 V the device starts to operate in impact mode and the power output increases by a factor of two.

The charging time of the energy storage capacitor was about 10 s for different load resistances.

Further work will involve comparison of the triangular electrode geometry, which combines area-overlap and gap-closing characteristics, to the linear geometry (area-overlap) in order to reveal advantages and disadvantages of the triangular geometry. Also, the efficiency of the rectification will be investigated with respect to both electrode geometries.

REFERENCES

[1] Mitcheson P D, Sterken T, He C, Kiziroglou M, Yeatman E M and Puers R 2008 Electrostatic Microgenerators *Measurement + Control* **41** pp 114-119

[2] Naruse Y, Matsubara N, Mabuchi K, Izumi M and Suzuki S 2009 Electrostatic micro power generation from low-frequency vibration such as human motion *J. Microeng. Micromech.* **19** 094002

[3] Hoffmann D, Folkmer B and Manoli Y 2009 Fabrication, characterization and modeling of electrostatic micro-generators *J. Microeng. Micromech.* **19** 094001

[4] Hoffmann D, Folkmer B and Manoli Y 2007 Design considerations of electrostatic electrode elements for in-plane micro-generators *Proc. PowerMEMS 2007* 15-18